Corrosion resistance and biocompatibility of zirconium oxynitride thin film growth by rf sputtering

G.I. Cubillos
Departamento de Química, Universidad Nacional de Colombia, AA 14490, Bogotá- Colombia.

J.J. Olaya
Facultad de Ingeniería, Universidad Nacional de Colombia, AA 14490, Bogotá- Colombia.

D. Clavijo
Facultad de Medicina, Universidad Nacional de Colombia, AA 14490, Bogotá- Colombia.
Facultad de Medicina Fundación Universitaria Sanitas, Bogotá-Colombia.

J.E. Alfonso
Departamento de Física Universidad Nacional de Colombia, AA 14490, Bogotá- Colombia.
e-mail: jealfonsoo@unal.edu.co

M. Bethencourt
Departamento de Ciencia de los Materiales e Ingeniería Metalúrgica y Química Inorgánica.
Universidad de Cádiz. Centro Andaluz de Ciencia y Tecnología Marinas. Avda República de Saharaui.
Puerto real, E-11510. Cádiz- Spain.

Recibido el 23 de noviembre de 2011; aceptado el 16 de mayo de 2012

Thin films of zirconium oxynitride were grown on common glass, silicon (100) and stainless steel 316 L substrates using the reactive rf magnetron sputtering technique. The films were analyzed through structural, morphological, and biocompatibility studies. The structural analysis was carried out using X-ray diffraction (XRD), and the morphological analysis was carried out using scanning electron microscopy (SEM) and atomic force microscopy (AFM). These studies were done as a function of growth parameters, such as power applied to the target, substrate temperature, and flow ratios. The corrosion resistance studies were made on samples of stainless steel 316 L coated and uncoated with Zr_xN_yO films, through of polarization curves. The studies of biocompatibility were carried out on zirconium oxynitride films deposited on stainless steel 316L through proliferation and cellular adhesion. The XRD analysis shows that films deposited at 623 K, with a flow ratio $\Phi N2/\Phi O_2$ of 1.25 and a total deposit time of 30 minutes grew preferentially oriented along the (111) plane of the zirconium oxyitride monoclinic phase. The SEM analyses showed that the films grew homogenously, and the AFM studies indicated that the average rugosity of the film was 5.9 nm and the average particle size was 150 nm. The analysis of the corrosion resistant, shows that the stainless steel coated with the film was increased a factor 10. Finally; through the analysis of the biocompatibility we established that the films have a better surface than the substrate (stainless steel 316 L) in terms of the adhesion and proliferation of bone cells.

Keywords: Ziconium oxynitride; thin films; bone cells; biocompatibility.

PACS: 81.15.Cd; -87.68.+z; -68.43.-h

1. Introduction

Biomaterials are important in the development of biomedical devices and implants. The surface of the biomaterial is the first thing to contact the living tissue when the material is placed in the body. Therefore, the initial response of the living tissue to the biomaterial depends on the surface properties. Currently, it is rare that a biomaterial with good bulk properties also possess the surface characteristics suitable for some clinical applications. For that reason, over the last few years, the development of surface modification techniques for biomaterials has been expanding rapidly. In this way, it is possible to make ideal biomaterials with surface attributes that are decoupled from the bulk properties. For instance, by altering the surface functionality through the deposition of a thin film, the optimal surface, chemical, and physical properties can be attained.

For the foregoing reasons, thin films of metal such as Ti and alloys (Ti6Al4V and AISI 316 L steel) have been used in biomedical applications [1-3]. In these biomedical applications, during the last few decades Ti and its oxides have been the materials most widely used, because they have a high anticorrosive resistance within the aggressive environment of the body; however, nowadays research is being carried out that seeks to increase the lifespan of the prosthesis through processes of proliferation and adhesion of bone cells on thin films of, for example, niobium, zirconium and tantalum and its oxides [3].

Taking advantage of the fact that the surface characteristics are relevant for the interaction between the implant and the living tissue [4–5], we proposed to make use of thin film technology to modify any base material with a biocompatible coating. The coating material would be ceramic, such as zirconium oxynitride (ZrO_xN_y), a material that can be easily and inexpensively produced through thin film deposition techniques.

The growth of oxynitride films is strongly influenced by the amount of oxygen molecules and nitrogen present in the

deposition chamber. This influence has been studied by Martin *et al.* [6], who deposited TiN_xO_y using the pulsing gas technique and found that the chemical composition, structural evolution, and electrical response varies as a function the values of x and y. The techniques most commonly used to prepare oxynitride films are reactive rf, dc magnetron sputtering, and cathodic reactive arc evaporation [7].

The purpose of the present study is to evaluate the biocompatibility of zirconium oxynitride thin films deposited on stainless steel, using reactive rf magnetron sputtering through the analysis of the proliferation and adhesion of bone cells.

2. Experimental techniques

2.1. Growth of the ZrN_xO_y films

The equipment used to grow the ZrN_xO_y films was an Alcatel HS 2000 described in previous papers [8]. The ZrN_xO_y films were obtained from a 4"×1/4" Zr (99.9%) target (CERAC, Inc.). The parameter set used during deposition process was: base pressure (2.0×10^{-3} Pa), total working pressure (7.4×10^{-1}Pa), and deposition time (half hour), target–substrate distance (5 cm), argon (99.999%) flow (20 sccm). We studied the influence of several deposition parameters such as: power supplied to the target (from 200 to 350 W), substrate temperature (which varied from 287 to 623 K), and flow ratios (1.0, 1.25 and 1.50) of N_2 (99.99 %) and O_2 (99.99 %) in same ratios inside the deposit chamber. The final working pressure was maintained using a valve controller for all the ratio flow values given above. The temperature of the substrate was measured with thermocouple type K, and the argon, nitrogen and oxygen flows were controlled with mass flow controllers. The structural characterization of the films was performed through XRD with a Philips diffractometer operated at 30 kV and 20 mA, working in Bragg-Brentano configuration and using Cu Kα radiation. The average crystalline size was calculated from s=0.9 k/Bcosθ where B = $B_m - B_i$, B_m being the broadening of the diffraction line, measured full width at half maximum (FWHM) and B_i the instrument peak width[9]. Surface morphology was characterized by imaging the secondary electrons with a Quanta 2000 scanning electron microscope operating at 15 kV and 10 mA and non-contact AFM Autoprobe cp Park Scientific instrument with study area of 25 μm^2 and frequency of 10 Hz.

2.2. Corrosion Tests

The corrosion resistance of zirconium oxynitride coatings and stainless steel 316 L was evaluated through means of electrochemical techniques of potentiodynamic polarization and polarization resistance in a solution of NaCl at 3.5% (pH=6.5). Measurements were made in a K 235 flat cell of Parc EG&G using a Solartron SI 1287 potentiostat the reference electrode used was a Ag/AgCl electrode of Crison 0.207 mV/SHE with exposed area of 1.00 cm^2.

The activity of the samples of stainless steel 316 L and zirconium oxynitride coatings in the solution of NaCl was analyzed from the value of the polarization resistance, Rp. The degree of protection was evaluated by comparing the value of this resistance with that corresponding to a bare sample.

In the corrosion test, the polarization in the anodic region was evaluated in order to determine the corrosion resistance of the ZrN_xO_y film, and the polarization resistance (Rp) was calculated through the Simonds and Larson method [16-17], where Rp is the slope of the obtained curve of the graphic voltage vs density current; the equation that allows calculating Rp is that of Stern-Geary [18-19].

$$Rp = \frac{B}{i_{\text{corr}}} = \frac{BnF}{\nu_{\text{corr}}} \tag{1}$$

where B is the proportionality constant between polarization resistance and the current density, i_{corr} is the current corrosion, n is the number of electrons transferred during the corrosion process, F is Faraday constant, and v_{corr} is the potential corrosion.

2.3. Biological Tests

Bone lineage cells from nursing mice were suspended in a 1:1 solution of DMEM (Dulbecco's Modified Eagle's Medium) supplemented with fetal bovine serum 10%, 100 U/mL penicillin, streptomycin 100 mg/mL, 0.25 mg/mL amphotericin B, 10 mM beta-glycerophosphate, L-ascorbic acid-2-phosphate 100 uM, and dexamethasone 10 nM. This was centrifuged at 1200 rpm for 10 minutes, and the precipitate was suspended in 1 mL of the medium described. The solution was transferred to a well of 35 mm^2 with an additional 1 mL of medium and transferred to the incubator at 310 K and an atmosphere of 5% CO_2 in order to allow cell adhesion. After 48 hours, there was 100% confluence, and the first cell passage was made. Stainless steel samples with and without coating were sterilized by autoclaving for 30 minutes at 423 K and placed in plates of six wells, and 10,000 cells were added, obtained from the first passage, suspended in the medium described. These samples were incubated at 310 K and an atmosphere of 5% CO_2. When cell confluence was obtained, samples were extracted from the culture medium and washed three times with PBS (Phosphate Buffer Solution) at 310 K. The PBS solution was discarded, and the samples were immersed in 2 mL of 2.6-diamidine-2-phenylindole (DAPI) (SIGMA D9542) at a concentration of 1 mg/mL at 277 K. After 12 hours, the samples were removed and washed three times with PBS at 277 K in order to be deposited on glass slides.

DAPI-stained cells on coated and uncoated stainless steel were observed using fluorescence confocal microscopy (NIKON C1-Plus) and were captured in photographs. For image analysis, a series of algorithms was used, which were merged into the program Matlab (image toolbox) in order to transform the original color images to grayscale and apply algorithms and image processing (segmentation, threshold and filtering) in order to reduce the noise.

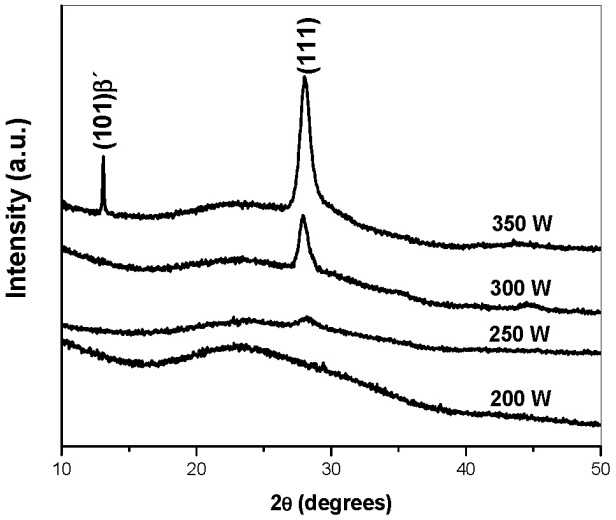

FIGURE 1. XRD patterns recorded from ZrN_xO_y films deposited on common glass substrate at 623 K, 2.0 sccm of oxygen and 2.5 sccm of nitrogen flows and at different powers.

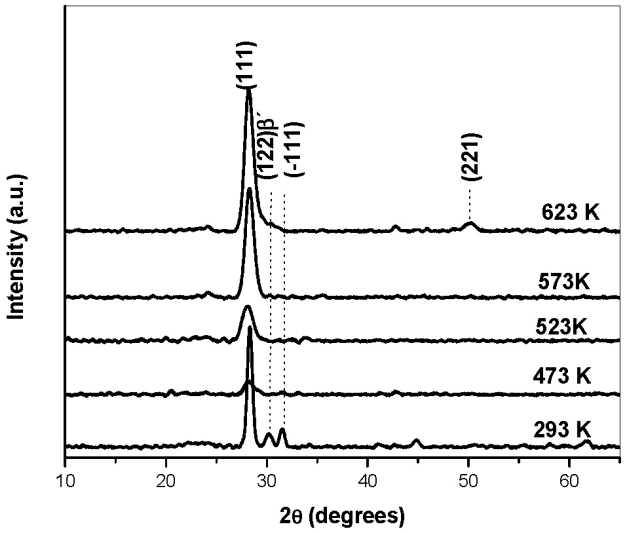

FIGURE 2. XRD patterns recorded from ZrN_xO_y films deposited on common glass substrate at 350 W, 2.0 sccm of oxygen and 2.5 sccm of nitrogen flows and at different substrate temperatures.

To do the cell counting, conventional border detection was performed, and the regions with the cells to be studied were identified, considering the edges and the fixed threshold. Two masks were applied, binary gradient and expansion gradient, obtaining binary images, segmented and linearized with threshold contrast for labeling the cells, in order to determine their distribution and number.

3. Results and discussion

3.1. Structural and morphological analysis of ZrN_xO_y thin films

X-ray analysis was carried out to determine the evolution structure of the ZrN_xO_y films as a function of the different parameters of growth. Figure 1 shows the XRD pattern of the ZrN_xO_y thin films grown at 623 K and with different power supplied to the target and by keeping constant the ratio between N_2 and O_2 at 1.25". The study of XRD established that the films evolved from an amorphous phase (200 W) on monoclinic polycrystalline film (350 W), which has two planes, the first one located at 12.96° and the other located at 27.94°. The first plane has been reported by Mazzoni *et al.* [10] as (101) plane of the β' phase of the $Zr_7O_{11}N_2$ (PDF 48-1637) and the second is the (111) plane belonging to monoclinic phase of the ZrO_2(PDF 720597). Films grown under 300 W only present the (111) plane associated with the same crystalline phase.

Another parameter of growth studied was the influence of the temperature of the substrate on the crystalline structure of the ZrN_xO_ythin films. Figure 2 shows the XRD pattern of the ZrN_xO_y thin films prepared at 350 W and at different temperatures of the substrate (N_2/O_2 ratio is 1.25) In the figure it is possible to observe that the films that were grown at room

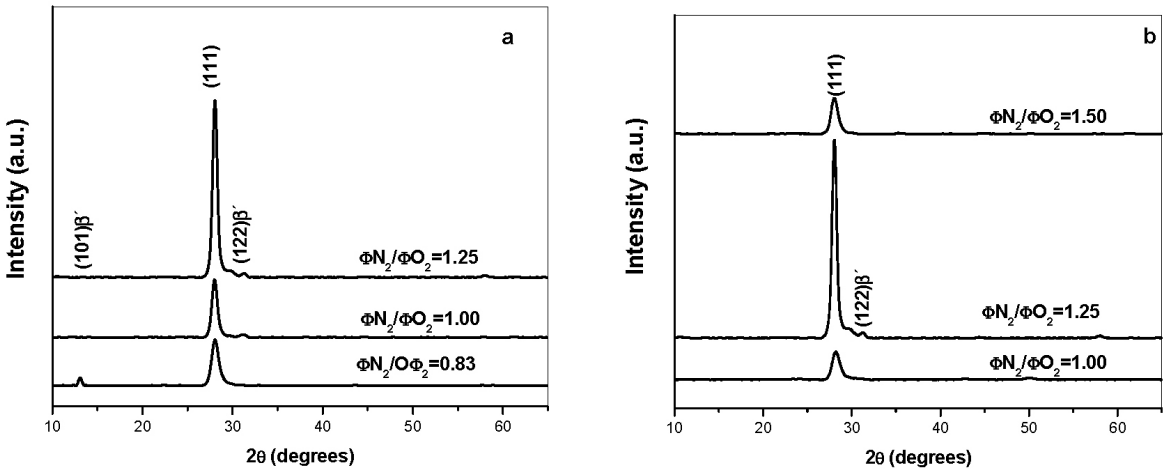

FIGURE 3. XRD patterns recorded from ZrN_xO_y films deposited on common glass substrate at 350 W, 623K and different flow ratio. a- flows of N_2 at 2.5 sccm and different oxygen flows, and b- - flows of O_2 at 2.0 sccm and different nitrogen flows.

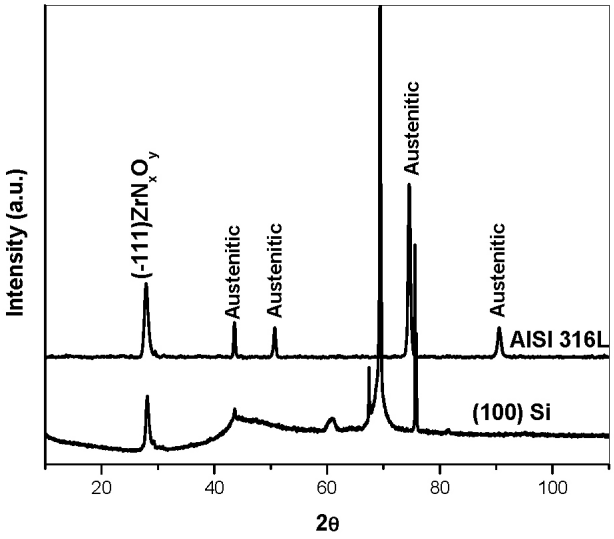

FIGURE 4. XRD patterns recorded from ZrN_xO_y films deposited on (100) Si and stainless steel AISI 3l6L substrates at 350 W, 623 K and flow ratios of 1.25.

temperature have a polycrystalline structure of the monoclinic phase, with growth preferentially along the (111) plane. Increasing the temperature on the substrate, the films acquire a basically mono-crystalline structure along the (111) plane. These results can be explained through an energy model [11-12], $i.e.$ increasing the power on the target as well as the substrate temperature results in increased energy of the ions that bombard the substrate and improvement of the mobility of the adatoms (zirconium, oxygen and nitrogen) in the substrate, thus obtaining thin films with high crystallinity.

Finally, the influence of the reactive gas flow ratios on the crystalline structure of the ZrN_xO_y films was studied. Figures 3a and 3b show the XRD patterns of the films where the flow ratios ($\Phi N_2/\Phi O_2$) have been changed, keeping the nitrogen or oxygen flow constant, respectively. Figure 3a shows that films grown at higher flow ratios have higher degrees of crystallinity. Figure 3b shows basically the same results as Fig. 3a, with the exception that with the films grown with higher flow ratios the crystallinity has decreased. Also, it is important to state that films grown with flow ratios of less than one showed an amorphous phase. These results indicate that the mean free path for ions of zirconium, nitrogen and and oxygen is greater for small flows of oxygen and nitrogen, which allows obtaining high degrees of crystallinity in the films grown.

In other studies, ZrN_xO_y thin films have been grown with flow ratios higher than that used in this paper; these studies

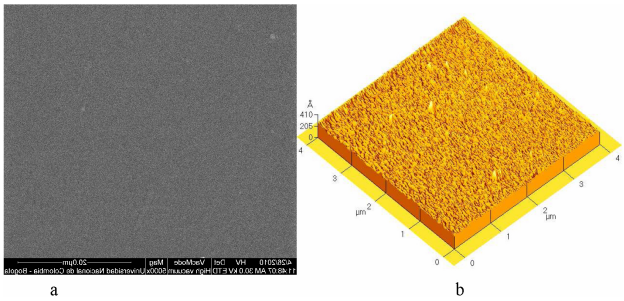

FIGURE 5. SEM micrograph ZrN_xO_y thin film morphology. b) AFM Micrograph the ZrN_xO_y film, deposited at 350 W, 623 K and flow ratio of 1.25.

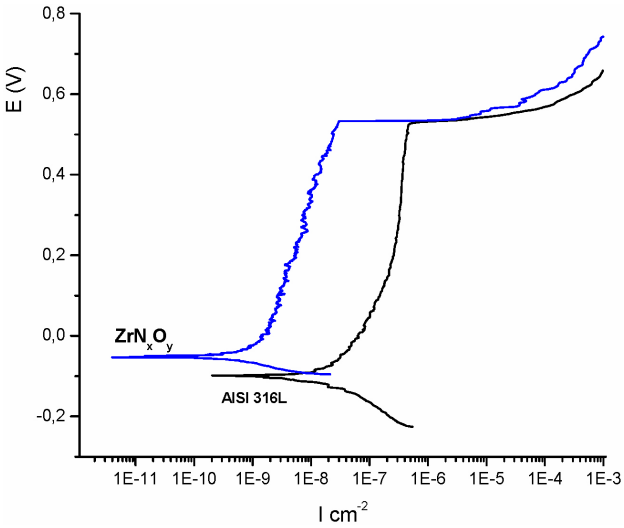

FIGURE 6. Linear polarization curves corresponding to samples tested in NaCl 3,5% solution

ies showed polycrystalline films with three mixed crystallographic structures: cubic, tetragonal and monoclinic [13].

To verify reproducibility of the deposit parameters on different substrates, ZrN_xO_y films were deposited on Si (100) and stainless steel AISI 3l6L. Figure 4 shows the XRD patterns in both substrates; in this figure only the (111) plane belonging to the monoclinic phase of ZrN_xO_y is shown, confirming results obtained on the common glass substrates.

On the other hand, with the expression to calculate the average crystalline size (see Sec. 2), we have established that along the (111) plane of the ZrN_xO_y films deposited at 350 W, 623 K and flux ratio of 1.25 the crystalline size is 20 nm. These results differ from those reported by Sushant *et al.* [14], who obtained an average crystalline size of 12 nm on ZrN_xO_y deposited at different partial pressures of oxygen.

TABLE I. Values of the parameters of the corrosion test.

Muestra	R_P (Ωcm^2)	E_{corr}(V)	I_{corr} A cm^{-2}	$E_{pitting}$(V)
316 L	1.235×10^6	-0.101	2.11×10^{-8}	0.528
316l - ZrN_x0_y(a)	1.54×10^7	0.2014	1.69×10^{-9}	0.546
316 L -ZrN_xO_y(b)	1.93×10^7	0.185	1.35×10^{-9}	0.607

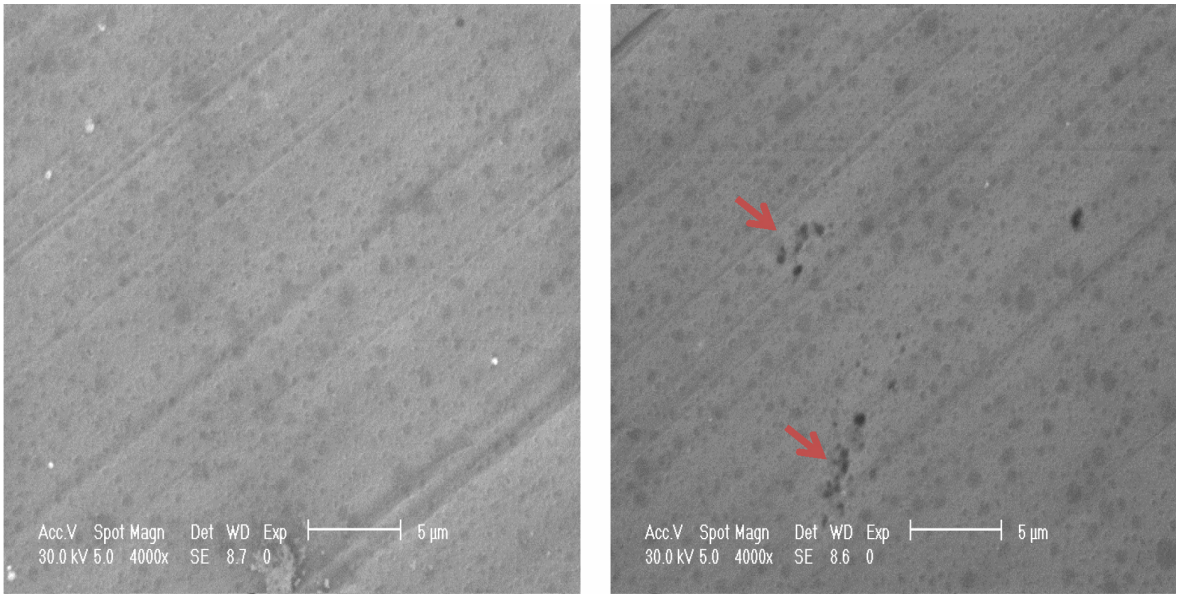

FIGURE 7. a) SEM micrograph the morphology of ZrN_xO_y thin film before polarization. b) after polarization in NaCl 3,5%, deposited at 350 W, 623 K and flow ratio of 1.25.Steel 316L coated with ZrNxOy film.

The results of the morphology carried out through the SEM study (Fig. 5a) on ZrN_yO_xfilms that were deposited at optimal conditions (350 W of power, substrate temperatures of 623 K and flow ratios of 1.25) $i.e$ those that reached the highest degree of crystallinity, show a highly homogenous surface that may be very compact. In this it is not possible to find contrast and therefore the growth mechanism is not defined The microstructure of the films was evaluated through AFM studies (Fig. 5b). The AFM micrograph reveals that the average grain size was 150 nm [9] with an average rugosity of 59 nm.

4. Study of the corrosion resistance of ZrN_xO_y thin films

The study of the corrosion resistance both the stainless steel coated with ZrN_xO_y film and the substrate (316 AISI stainless steel) were made through anodic and linear polarization test using a NaCl (3.5%) solution. Fig. 6 shows Tafel plots obtained for a stainless steel substrate and ZrNxOy coating deposited with 350 W, 623 K and ratio reactive gases flows of 1.25. Table I summarizes that the corrosion of ZrN_xO_y coating compared to the substrate, showed more positive values and lower corrosion current density, attaining up to three orders lower magnitude compared with the bare substrate. These results show that the ZrN_xO_yfilm allows increase the corrosion resistance. Similar results have been obtained by Ariza *et al*., who has deposited ZrN_xO_y films over stainless steel used to tools type M2 [14,15] and has made corrosion test in an artificial sweat solution (pH= 4.5).

The Rp values (Table I) were obtained from the lineal polarization curve that allowed confirming that the film of ZrN_xO_y increased in approximately 13.5 times the resistance corrosion of the stainless steel. The values of pitting potential and passivation zone are no different to the obtained to the stainless steel. The superficial morphology of the ZrN_xO_y film before and after of corrosion test (Fig. 7a and 7b) allows understood this behavior. After the test the corrosion appear pitting (see arrows in Fig. 7b) which evidence that the corrosive solution permeates the film and reaches the surface of the steel. The barrier properties of the ZrN_xO_y coatings, depend on the microstructure and interfacial adhesion. For PVD coatings, the inter-columnar space, the micro and nano-pores (pinholes) and possible micro cracks allow the diffusion of the NaCl electrolyte toward the substrate, leading to corrosion of the substrate and film delamination. Also this phenomenon can be explained by galvanic coupling produced by the difference between the corrosion potential of the ZrO_xN_y thin film and uncoated areas. The potential difference is characterized by anodic dissolution of the substrate material with a high anodic current density at defect site, leading to an adhesion failure of the coating.

4.1. Study of the biocompatibility of the ZrN_xO_y thin films

In order to establish the impact that the ZrN_xO_y thin film has on the adhesion and the proliferation of bone cells, we deposited bone cells on stainless steel both covered with ZrN_xO_y film and without film. The growth and morphology of bone cells that were previously deposited on stainless steel were determined through optic microscopy. Figure 8a shows the optical micrograph of the proliferation of bone lineage cells at the edges of the samples of untreated steel 316 L, and the Fig. 8b shows steel 316 L coated with ZrN_xO_y film, at 72 hours of culture. Neither of the two samples shows inhibition of cell proliferation along the edges.

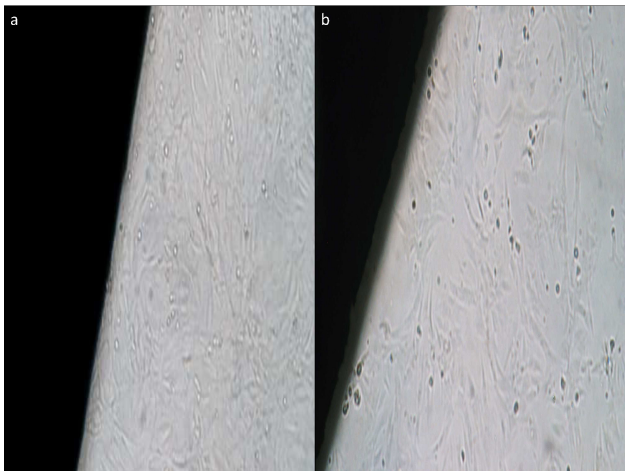

FIGURE 8. Optical micrograph of the proliferation of bone lineage cells at the edges of the samples a-uncoated steel 316L and b- steel 316L coated with ZrN_xO_y film at 72 hours of culture.

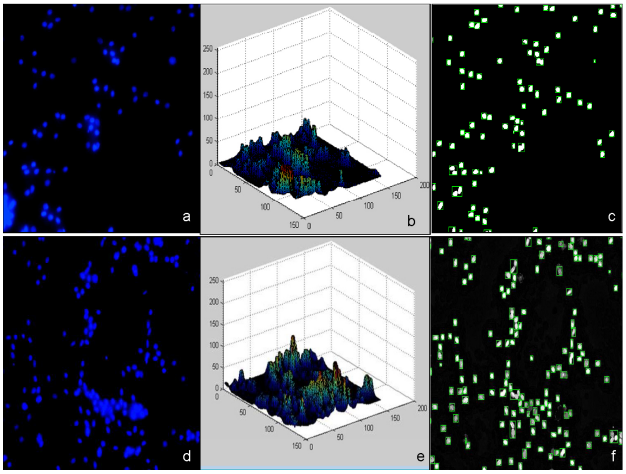

FIGURE 9. Image Processing: image distribution, models 3D cells and threshold for stainless steel 316L (a, b and c) without film of ZrN_yO_x and stainless steel 316L with ZrN_xO_y film (d, e and f).

Figure 9 shows images of fluorescence microscopy with a filter, taken of bone cells grown on stainless steel without film (Fig. 9a, and from the bone cell grown on stainless steel 316L coated with ZrN_xO_y film (Fig. 9d). Also is shows the threshold of the image that was used for counting bone cells (Fig. 9c and 9f, for steel uncoated and coated, respectively). To minimize error in the information recorded (clusters of cells that the program could detect as a single cell), standard-size cells were taken as a reference and reduced to a minimum of noise, and thus data is obtained within a degree of error of 1-2%.

The cell number under analysis by segmentation and threshold algorithms for monochrome images based on the discontinuity and/or similarity of the intensity values in images was 93 for the image of stainless steel 316 L without ZrN_xO_y film and 153 on stainless steel 316 L with a film of ZrN_xO_y. These results indicate that the stainless steel coated with a ZrN_xO_y thin film promotes the adhesion of the bone lineage cells, facilitating their proliferation.

5. Conclusions

In this study ZrN_xO_y thin films were deposited as a function of the deposit parameters, and under our experimental conditions it was found that the best conditions to obtain thin films with mono-crystalline structure along the (111) plane of monoclinic ZrN_xO_y phase were: 350 W, 623 K and flow ratios of 1.25.

The films deposited at these conditions on stainless steel 316 L were evaluated through the corrosion test and biocompatibility response of bone cells deposited on them. The study of the corrosion showed that the film of ZrN_xO_y increase the Rp in about 13.5 times of the stainless steel 316 L; the test of biocompatibility showed that the bone linage cells increased their adhesion and proliferation by about 64 % when the stainless steel 316 L is coated with a ZrN_xO_y thin film. The adhesion and cell proliferation are essential for osseointegration in the tissue-biomaterial interface.

Acknowledgments

The authors would like to aknowledge the finalcial support given to this project by division de investigación de la Universidad nacional de Colombia under grant No 11842.

1. E. Eisenbarth, M. Muller, R. Thull, D. Velten, and J. Breme, *J. Biomed. Mater. Res. Part A*, **79** (2006) 166-175.
2. H. Matsuno, A. Yokoyama, F. Watari, M. Uo and T. Kawasaki, *Biomaterials* **22** (2001) 1253-1262.
3. E. Eisenbarth, D. Velten, M. Muller, and R. Thull, *J. Breme. Biomateriales* **25** (2004) 5705-5713.
4. D.G. Castner and B.D. Ratner, *Biomedical surface science: Foundations to frontiers. Surf. Sci.* **500** (2002) 28-60.
5. B.D. Ratner, *Biosens. Bioelectron*. **10** (1995) 797-804.
6. N. Martin *et al.*, *Appl. Surf. Sci.* **185** (2001) 123–133
7. S.H. Mohamed, A.M.A. El-Rahman, and M.R. Ahmed, *J. Phys. D: Appl. Phys.* **40** (2007) 7057–7062.
8. J.E. Alfonso, J. Torres, J.F. Marco, *Brazilian J. Phys.* **36** (2006) 994.
9. B.D. Cullity, *Elements of X-ray Diffraction* second ed. (Addison-Wesley, London 1978) p. 102.
10. A.D. Mazzoni, M.S. Conconi, E.F. Aglietti, *Mat. Res.* **4** (2000) 107-111.

11. B.A. Movchan and A.V. Demchishin, *Fiz. Met. Metalloved.* **28** (1969) 83.
12. R. Messier, A.P. Giri, R.A. Roy, *J. Vac. Sci. and Tech. A.* 2(2, Pt. 1), 500-3.
13. M. Laurikaitis, S. Burinskas, J. Dudonis, and D. Milèius, *J. of Phys.: Conference Series 100* (2008) 08205.
14. K. Rawal Sushant, A. Kumar Chawla, V. Chawla, R. Jayaganthan, and R. Chandra, *Mat. Sci. and Eng. B* **172** (2010) 259–266.
15. S.C. Ferreira *et al*., *Surface & Coatings Technology* **200** (2006) 6634–6639.
16. E. Ariza *et al*., *Thin Solid Films* **469–470** (2004) 274–281.
17. E.J. Simmons, *Corrosion* **11** (1955) 255.
18. R.V. Skold and T.E. Larson, *Corrosion* **13** (1964) 139.
19. M. Stern, *Corrosion* **14** (1958) 329.
20. M. Stern, *Corrosion* **14** (1958) 440.